forests

MDPI

Article

Unveiling the Potential of Brazilian Eucalyptus for Transparent Wood Manufacturing via the Kraft Pulping Process as a Future Building Material

Kelvin Techera Barbosa [1,*], Gabriel Valim Cardoso [2], Andrey Pereira Acosta [3], Arthur Behenck Aramburu [1], Rafael de Avila Delucis [4], Darci A. Gatto [4], Jalel Labidi [5,*] and Rafael Beltrame [4]

1 Postgraduate Program in Mining, Metallurgical and Materials Engineering, Federal University of Rio Grande do Sul, Porto Alegre 91501-970, RS, Brazil; arthuraramburu@gmail.com
2 Wood Industrial Engineering, Engineering Center, Federal University of Pelotas, Pelotas 96010-900, RS, Brazil; gabriel.valim.cardoso@gmail.com
3 Postgraduate Program in Materials Science and Engineering—PIPE, Federal University of Paraná, Curitiba 80035-060, PR, Brazil; andrey.acosta@ufpr.br
4 Postgraduate Program in Materials Science and Engineering, Federal University of Pelotas, Pelotas 96010-900, RS, Brazil; rafael.delucis@ufpel.edu.br (R.d.A.D.); gattodarci@gmail.com (D.A.G.)
5 Environmental and Chemical Engineering Department, University of the Basque Country UPV/EHU, Plaza de Europa 1, 20018 San Sebastián, Spain
* Correspondence: kelvintecherabarbosa@gmail.com (K.T.B.); jalel.labidi@ehu.eus (J.L.)

Abstract: The emergence of transparent wood as a viable alternative to traditional glass has sparked considerable interest in recent research endeavors. Despite advancements, challenges persist in the delignification methods and wood species utilized in prior studies. Therefore, this study delves into the potential of Brazilian eucalyptus wood for transparent wood production through the kraft pulping process. Delignification was carried out in a laboratory setting, replicating the kraft process with varying reaction times (15, 30, 45, and 60 min). The resulting delignified wood veneers were impregnated with a pre-polymerized PMMA solution. The study encompassed various analyses, including UV-Vis spectroscopy, colorimetry, SEM, optical microscopy, and mechanical property evaluations. The results revealed intriguing trends in terms of transparency, color changes, microstructural modifications, and mechanical properties as a function of delignification time. This work presents valuable insights into the transformative potential of eucalyptus wood, offering a deeper understanding of the interplay between wood modification and PMMA impregnation.

Keywords: lignin removal; delignification; optical properties; bio-composite; polymethyl methacrylate; wood modification

Citation: Barbosa, K.T.; Cardoso, G.V.; Pereira Acosta, A.; Aramburu, A.B.; Delucis, R.d.A.; Gatto, D.A.; Labidi, J.; Beltrame, R. Unveiling the Potential of Brazilian Eucalyptus for Transparent Wood Manufacturing via the Kraft Pulping Process as a Future Building Material. *Forests* **2024**, *15*, 1544. https://doi.org/10.3390/f15091544

Academic Editor: Zeki Candan

Received: 30 July 2024
Revised: 28 August 2024
Accepted: 29 August 2024
Published: 2 September 2024

1. Introduction

Transparent wood has attracted significant attention in recent years due to its potential applications in areas such as smart windows, building facades, and even solar cells [1–4]. Compared to traditional glass materials, transparent wood offers several advantages as it is derived from a renewable resource, which makes it a sustainable alternative to conventional building materials. Hu et al. [5] examined the carbon dioxide (CO_2) emissions associated with the Chinese container glass industry, categorizing them based on combustion, raw material decomposition, and the power and heat utilized by the enterprise (indirect emissions). Their simulation findings revealed an average of 0.69 tonnes of CO_2 emissions per tonne of glass product due to combustion, a notably higher figure compared to the European container glass industry's 0.46 tonnes of CO_2 emissions per tonne of glass product as reported by Zier et al. [6]. Its relatively high transparency and low opacity, achieved by adapting the microstructure and chemical composition of the wood (achieved by removing or altering

the lignin and impregnating it with an amorphous polymer), make it an attractive alternative to conventional materials such as glass in architectural applications, as well as being more energy efficient, providing better insulation properties, and potentially reducing artificial energy consumption [7]. However, it is important to mention that transmittance and haze (forward-scattered light) are commonly reported in the literature as characteristics to be improved in transparent woods [8,9]. Moreover, it boasts high durability and resistance to shattering, making it a safer choice for construction applications. Despite the use of a fossil-based polymer in the production of transparent wood, during its wood growth, the tree captures the CO_2 produced during the synthesis of the polymer itself, thus creating a closed cycle. Fully bio-based transparent wood materials have already been reported in the literature [10]. Transparent wood is, therefore, derived from a renewable resource, which makes it a sustainable alternative to conventional building materials [11].

The manufacturing of transparent wood involves removing lignin from the wood veneer through a chemical method that preserves the fiber structure. Delignification is a critical step as lignin contributes to 80%–95% of the light absorption in wood, impeding its transparency [12]. By selectively removing lignin, the resulting wood retains its structural integrity while allowing light to pass through. The delignified wood is then impregnated with a translucent polymer, enhancing its transparency [4,13] and creating a material that combines the strength and natural esthetics of wood with the light-transmitting properties of glass. This innovative process opens up new possibilities for applications in architecture, design, and renewable energy [14,15].

In addition, as the chromophore groups present in lignin are predominantly accountable for its brownish color and light-absorbing characteristics observed in natural wood, recent studies have highlighted an alternative approach to delignification by focusing on modifying the chromophoric composition of lignin, rather than completely removing lignin [12,16,17]. For instance, Li et al. [12] demonstrated the development of transparent wood by preserving the lignin content and employing an alkaline H_2O_2 hydrothermal solution to selectively eliminate lignin chromophores, thereby reducing processing time.

Various methods utilizing different reagents for lignin removal have been studied. Zhu et al. [18] successfully removed lignin from a Tilia wood using a solution of sodium hydroxide (NaOH) and sodium sulfite (Na_2SO_3), resulting in a lignin content of 3%. Similarly, Qin et al. [19] and Wu et al. [20] investigated the use of $NaClO_2$, achieving residual lignin contents of 7% and 9%, respectively, for transparent wood production. However, the use of chlorine-based delignification processes leads to the formation of toxic effluents, increased time and energy consumption, and atmospheric pollution [19].

Based on this concept, using a consolidated process in the wood industry such as the kraft process and an abundant eucalyptus wood with a production of 38.9 m^3/ha/year [21], combined with a commonly used polymer, shows the possibility of the mass production of transparent wood on a pilot scale. The kraft process, widely utilized in pulp and paper industries, involves cooking wood with sodium hydroxide (NaOH) and sodium sulfide (Na_2S) to dissolve lignin and disaggregate fibers with minimal carbohydrate degradation [22]. Currently, the kraft process is the primary method for pulp production due to its continuous cooking process and the advantage of the associated chemical product recovery system [23,24].

Currently, the literature on transparent wood already encompasses studies involving woods delignified through the kraft process. For instance, Zhu et al. [25] reported the use of a process involving soaking wood blocks in a boiling solution containing NaOH and Na_2SO_3 to dissolve part of the lignin content, followed by a treatment with H_2O_2 to remove the remaining lignin. Hai et al. [26] conducted a similar study where hardwood kraft pulp underwent TEMPO-oxidation treatment followed by nanofiber fabrication. These examples highlight the existing research but emphasize the unique contribution of our study focusing on Brazilian eucalyptus in the context of transparent wood production.

In Brazil, the kraft process is employed with *Eucalyptus* sp., a fast-growing wood species that is crucial for pulp industries while simultaneously mitigating deforestation [27]. Eucalyptus species have been genetically manipulated for pulp production, resulting in fast-growing

wood with high productivity, cellulose content, and low lignin content and extractives. This makes it an ideal candidate for delignification processes [28,29]. Given these factors, there is a strategic importance in investigating the use of Brazilian eucalyptus wood for the production of transparent wood. Thus, this study aims to apply the kraft process with sodium hydroxide (NaOH), sodium sulfide (Na_2S), and hydrogen peroxide (H_2O_2) for the production of transparent wood from a Brazilian eucalyptus (*Eucalyptus grandis*).

2. Materials and Methods

2.1. Materials

Eucalyptus grandis wood veneers were obtained from Ecofolhas (São Paulo, Brazil). The density of the veneers was determined to be 0.44 g.cm^{-3} using a precision analytical scale (±0.01 g) and a digital caliper (±0.001 mm). Test specimens with dimensions of 20 mm × 20 mm × 0.6 mm (length × width × thickness, respectively) were prepared for the wood delignification process. All the specimens were stored in a climatic chamber at 20 °C and 65% relative humidity until reaching hygroscopic equilibrium (12% moisture content).

The chemicals used in the experiment were sodium hydroxide (NaOH) with a molar mass of 40.00 g/mol; sodium sulfide (Na_2S) with a molar mass of 78.04 g/mol; ethanol (C_2H_6O); hydrogen peroxide (H_2O_2) with a purity of 35%; methyl methacrylate (MMA) with a purity of 99%, a liquid state, and a molar mass of 100.12 g/mol; and a benzoyl peroxide catalyst, all of which were acquired from Sigma Aldrich (St. Louis, MO, USA).

2.2. Wood Delignification

The delignification process of the eucalyptus wood veneers was conducted by replicating the kraft process in the laboratory. The liquor–wood ratio was maintained at 4:1, and the active alkali conditions of 18% and sulfidity of 20% were achieved using NaOH (99.2 g/L) and Na_2S (36.27 g/L). The samples were treated with the delignification solution using four different delignification times (c.a. 15, 30, 45, and 60 min) and a temperature of 90 °C. Fibers started separating from each other after 60 min of kraft cooking; therefore, no tests were conducted beyond this time. The separation of the fibers probably occurred due to a significant breakdown of lignin and hemicellulose, crucial elements that bind fibers together within the wood structure. As the delignification process advances, these binding agents gradually lose their effectiveness, causing fibers to loosen and eventually separate from each other.

After the delignification process, the lignin-extracted samples were carefully rinsed with distilled water until reaching a neutral pH. Subsequently, the samples were immersed in a 35% hydrogen peroxide (H_2O_2) solution at 90 °C until the yellowish color of the samples was completely eliminated (around 2 h). Following the bleaching treatment, the samples were dehydrated by immersing them in pure ethanol P.A. (C_2H_6O) for about 60 min to allow the impregnation of the wood by the PMMA polymer. The nomenclatures assigned to the samples after the delignification are specified in Table 1.

Table 1. Nomenclatures used for delignified wood and their respective delignification time.

Delignified Woods	Nomenclatures
Delignified pristine wood for 15 min	DW15min
Delignified pristine wood for 30 min	DW30min
Delignified pristine wood for 45 min	DW45min
Delignified pristine wood for 60 min	DW60min

2.3. MMA Impregnation

MMA and benzoyl peroxide at a weight ratio of 98.5:1.5 were mixed to prepare the polymeric solution. The solution was heated at 70 °C for 15 min and then cooled in an ice bath at 10 °C until reaching room temperature, resulting in a pre-polymerization of the MMA solution. For wood impregnation, the delignified wood veneers were placed in Petri

dishes and covered with the pre-polymerized solution for 2 h. The polymer permeated the wood by capillarity at atmospheric temperature and pressure.

Afterward, the samples were wrapped in aluminum foil, placed between two metal plates to preserve their anatomical structure, and then placed in a forced air circulation oven at 75 °C for 4 h for complete MMA polymerization. After the polymerization, the transparent wood samples were removed from the oven. The nomenclatures of the samples after the polymerization are specified in Table 2.

Table 2. Nomenclatures used for delignified and subsequently impregnated wood with their respective delignification time.

Transparent Woods	Nomenclatures
MMA impregnated DW15min	TW15min
MMA impregnated DW30min	TW30min
MMA impregnated DW45min	TW45min
MMA impregnated DW60min	TW60min

2.4. Chemical Characterization

Wet chemical analyses were performed only for the pristine wood and for the delignified wood groups (DW15min, DW30min, DW45min, and DW60min) to analyze the effect of the kraft process in relation to the treatment time. The specimens were taken to a laboratory oven heated at 50 °C until reaching constant mass. After drying, the samples were grinded in a Willey mill and sieved in a 40-mesh sieve in accordance with T257 cm-12 [30]. Afterward, the ethanol–toluene extractives (Tappi T204 om-97 [31]), acid-insoluble (Klason) lignin (Tappi T222 om-98 [32]), ashes (T211 om-93 [33]), and holocellulose (remaining mass up to 100%) contents were determined.

Fourier transform infrared spectroscopy (FT-IR) was performed in order to characterize the structural chemical groups of the natural and the highest delignification groups. Thus, pristine wood, DW60min, and TW60min were analyzed using a 4100 equipment (Shimadzu Prestige 21 spectrometer equipped with ATR-8200), in which each spectrum resulted from 32 scans performed in the wavelength range of 4000 cm^{-1} to 400 cm^{-1} with a resolution of 4 cm^{-1}, scanner speed of 2 mm/s, and filter of 30.000 Hz filter.

2.5. Morphological Analyses

Morphological analyses were performed in the transverse and tangential planes using surface images obtained by an optical microscope (Rohs® mark, 2.0 resolution), wherein the images of pristine wood, delignified wood, and transparent wood were taken. The pristine wood and TW60min group were submitted to scanning electron microscopy (SEM) in a Phenon-World mark (Pro X model) with magnifications between 80 and 130,000 times (resolution $\leq$ 14 nm) to evaluate the MMA impregnation in the transparent woods. Finally, the light transmittance spectra were measured with a UV-Vis spectrometer (CARY 5000 Spectrophotometer) and the wavelength range was 400–800 nm. The tests were carried out in all the transparent wood groups in accordance with ASTM D1003 [34].

2.6. Thermogravimetric Analysis

A thermogravimetric analysis (TGA) was performed in the pristine wood, DW60, and TW60 groups in order to analyze the thermal behavior of the samples at the end of the treatment. A TGA-1000 equipment (Navas brand) was used, and the analysis was carried out with a heating rate of 10 °C-min^{-1} under an inert atmosphere and a nitrogen gas flow of 2 L-min^{-1}.

2.7. Color Measurements

Colorimetry was carried out to analyze the color change in the wood veneers due to the delignification time. Pristine wood and transparent wood groups color parameters

were measured with a UV-Vis spectrometer (CARY 5000 Spectrophotometer) following the CIEL*a*b* method used to measure the luminosity index (L*) and chromaticity parameters (coordinate (a*), coordinate (b*), and total color variation (ΔE)). Five readings were acquired by each group.

2.8. Surface Analysis

The surface roughness of pristine wood and transparent wood groups was evaluated using an Ambios XP-2 Mechanical Profilometer. Roughness (Surface Topography), 5 readings of average roughness (Rz, average distance between peak and valley), and (Ra, average roughness) per group were taken in the tangential plane. Five readings were acquired by each group.

Furthermore, surface hydrophobicity analysis was performed in order to evaluate surface repellence to water in the natural and transparent wood groups. Five samples per group were used, measuring the apparent contact angle at six different times, from 5 s to 60 s after water (a drop of 10 µL)/slide contact, using a Kruss DSA25 goniometer according to the sessile drop method. Five readings were acquired by each group.

2.9. Water Absorption

The hydrophobicity of the material was evaluated for the transparent wood group by the water repellency efficiency (WRE). Initially, the samples were oven-dried at 100 °C (to constant mass) to standardize the initial moisture condition. Five readings were acquired by each group.

The level of WRE of the transparent wood at different delignification times was measured during four immersion-drying cycles. In each cycle, the mass and volume of the samples were measured at zero time (the samples dried at 100 °C) and after 96 h of immersion. With the data obtained, the WRE was calculated by Equation (1).

$$\text{WRE} = ((\Delta M\ nt - \Delta M\ t)/(\Delta M\ nt)) \times 100\% \quad (1)$$

where ΔM = (Mu − Ms)/Ms where ΔM = mass change; Mu = wet sample mass (g); Ms = dry sample mass (g); t = treated; and nt = untreated.

2.10. Mechanical Properties

Tensile tests were carried out according to the ASTM D 638-10 [35] with adaptations to the dimensions of the test specimens, which were 70 mm × 20 mm × 0.6 mm. For that, 5 readings were acquired by each group using a Universal Mechanical Testing machine (DL500 Emic), with a load cell of 5 kN at a controlled speed of 5 mm/min. Tensile strength (σ_t) was calculated by dividing the maximum load sustained by the specimen by the average original cross-sectional area in the gage length. Percent elongation at break was determined by the change in gage length at the point of specimen rupture. The modulus of elasticity (E_t) was calculated by the linear portion of the load vs. displacement curve. Finally, the toughness was calculated by the area under the load vs. displacement curve.

2.11. Statistical Analysis

All the data were submitted to the one-way ANOVA analysis of variance, except for the contact angle. The homogeneity of the variances and normality of data were verified using the Shapiro–Wilk tests. Whenever the null hypothesis was rejected, Tukey's tests were used to compare the means, and all the statistical analyses were implemented at the 5% significance level.

3. Results and Discussion

3.1. Chemical Composition

Table 3 shows a significant increase in the ash content after the delignification processes, which can be attributed to the inorganic salts used in these treatments. These salts, such as NaOH and Na_2S, contribute to the removal of lignin from the wood, but they can also

introduce additional mineral content into the wood structure [36]. As a result, compared to the pristine wood, the other chemical quantities were all reduced in the delignified ones.

Table 3. Chemical composition of the eucalyptus wood prior to and post the delignification processes.

	Holocellulose (%)	Extractives (%)	Ashes (%)	Acid-Soluble Lignin (%)	Acid-Insoluble Lignin (%)
Pristine wood	69.52 ± 0.54 c	2.63 ± 0.25 ab	0.08 ± 0.05 a	1.16 ± 0.18 c	26.60 ± 0.27 e
DW15min	43.37 ± 1.53 a	2.05 ± 1.65 a	30.25 ± 0.08 b	0.34 ± 0.24 ab	23.98 ± 0.50 d
DW30min	44.36 ± 0.48 ab	2.55 ± 0.41 ab	30.96 ± 0.51 bc	0.23 ± 0.07 a	21.86 ± 0.89 c
DW45min	44.90 ± 2.37 ab	3.96 ± 0.77 bc	31.66 ± 0.64 c	0.69 ± 0.13 b	18.76 ± 1.72 b
DW60min	46.05 ± 1.22 b	5.06 ± 0.45 c	32.84 ± 0.37 d	0.58 ± 0.28 ab	15.46 ± 0.45 a

where different letters represent statistically different means.

When comparing the delignified woods, it is observed that the acid-soluble lignin content remained stable, while the extractives and holocellulose contents increased, and acid-insoluble lignin content decreased with the delignification time. These trends can be explained by the fact that during the delignification process, the treatment primarily targets the acid-insoluble lignin and, as a result, that acid-soluble lignin fraction is less affected and remains relatively stable throughout the process [37]. According to Jiang [38], the acid-insoluble portion of lignin is more easily dissolved and removed in an alkaline environment, as it reacts readily with the hydroxide ions (OH-) from NaOH, forming soluble alkali lignin compounds. These compounds can be washed away during the rinsing process, and the lignin becomes soluble in the alkaline medium. Additionally, the increase in the extractives and holocellulose contents can be attributed to the removal of lignin, which acts as a barrier, making these components more inaccessible for extraction [39,40].

Figure 1 displays the variation in both the percentage of removed lignin and the total lignin content (c.a. the sum of the soluble and insoluble lignin in acid). It can be observed that the lignin removal increased gradually with the delignification time, reaching 42.22% after 60 min. The achieved lignin contents can be considered higher than most of those found in the literature related to veneers intended for transparent wood manufacturing. After the hydrogen peroxide treatment, based on the literature, it is expected that lignin removal increase by approximately 15%, which may depend on some influencing factors, such as the concentration of hydrogen peroxide, treatment time, temperature, and the initial lignin content in the wood [41–43].

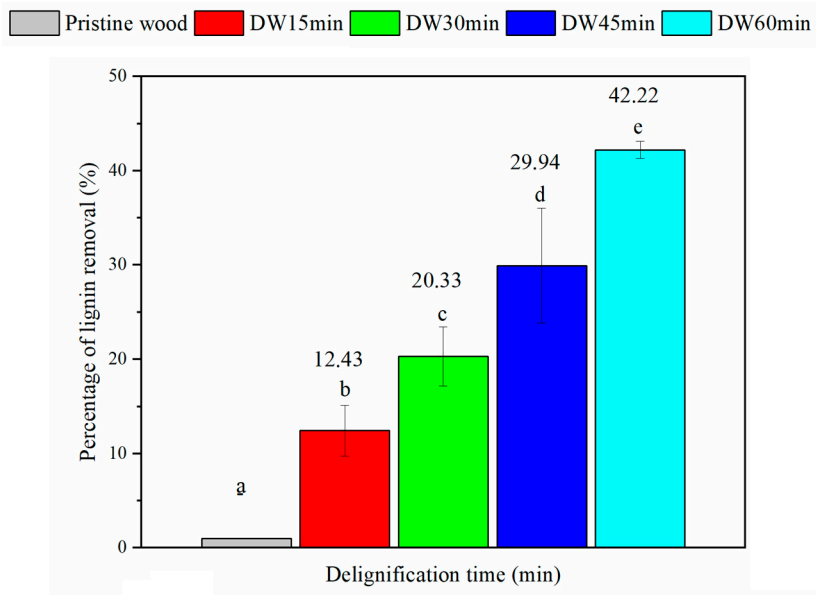

Figure 1. Percentage of lignin removal for the delignified wood veneers where different letters above the bars represent statistically different means.

It's important to highlight that eucalyptus wood requires careful consideration. As reported by Pinto et al. [44], at temperatures below 70 °C, about 20% of the lignin dissolves without major structural changes. However, when the temperature exceeds 70 °C, the lignin in the cell wall undergoes significant degradation and fragmentation before dissolving.

However, it is essential to note that the final lignin content of the delignified wood does not singularly dictate the final transparent wood properties. The other attributes of the delignified wood, such as the cellulose structure, pore characteristics, chemical composition, density, and the impregnation process [45,46], substantially impact the properties of interest in transparent wood. Therefore, the final properties of transparent wood may depend on various factors, including the lignin content, microstructure, chemical composition, presence of defects, processing conditions, impurities, and moisture content [20,47,48]. Despite this, the study conducted by Wu et al. [20] reported variation in the final lignin contents ranging from 9 to 24% for delignified Basswood (*Tilia*) veneers. This specific study employed a mixture of 2 wt% $NaClO_2$, 0.1 wt% glacial acetic acid, and 97.9 wt% ultrapure water. The dried samples underwent delignification in a water bath oscillator at 80 °C, with an oscillation frequency of 40 rpm, for different treatment durations spanning from 30 to 150 min.

3.2. FTIR Spectroscopy

Figure 2 displays the FTIR spectra of the original eucalyptus veneer, as well as the samples subjected to the 60 min delignification treatment (DW60min) and the subsequent impregnation with PMMA (TW60min). In addition to the peaks associated with the presence of carbohydrates at 1030 cm^{-1} (C-O-C stretching in cellulose) and 1730 cm^{-1} (acetyl groups in hemicelluloses) [46], the pristine wood exhibits absorption bands related to lignin, such as those near 1700 cm^{-1} (C=O stretching in lignin) [40] and 1200–1100 cm^{-1} (C-O stretching in lignin) [49].

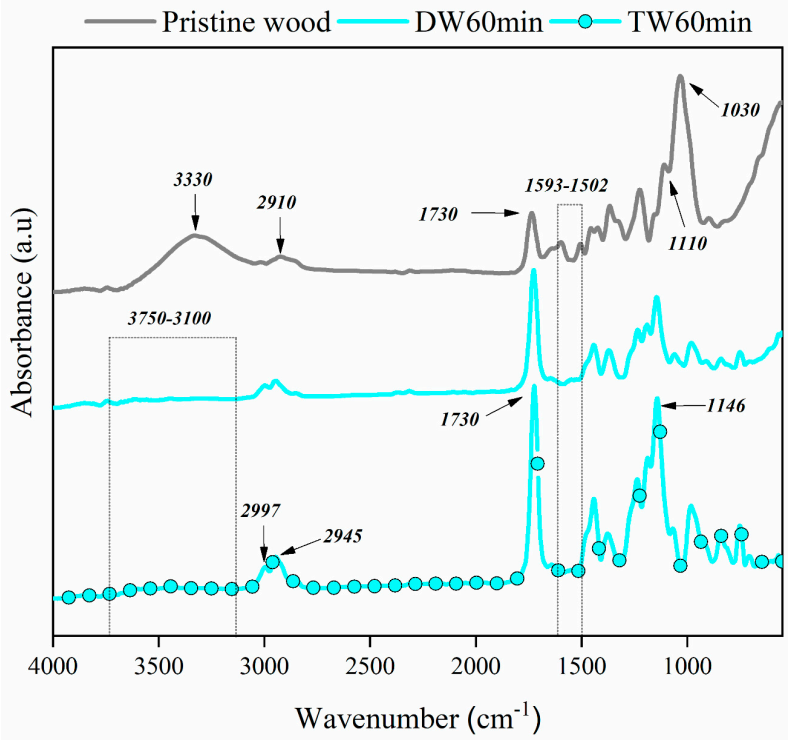

Figure 2. FT-IR spectra of a pristine wood, a delignified wood, and a transparent wood.

In comparison to the pristine wood, the modified samples exhibited a reduction at 1700 cm^{-1} and a disappearance of lignin-related absorption bands at 1500–1600 cm^{-1} as a result of the delignification process. The delignified sample (DW60min) also displayed alterations in absorbance at various wavenumbers corresponding to wood components due

to the delignification treatment, such as at 1510–1550 cm^{-1} (associated with C-H bending vibrations in lipid components and linked to C=C stretching vibrations in phenolic rings present in tannins and other phenolic compounds) [50].

Within the transparent wood (TW60min), there was an indication of PMMA-related absorption bands, including carbonyl stretching at approximately 1720–1730 cm^{-1} [47]. Additionally, newly emerged absorption bands associated with PMMA polymerization were detected at 2990 cm^{-1} (an increase in CH_3 stretching vibrations signifying the presence of methyl groups in the polymer structure) [47]. Furthermore, both the DW60min and TW60min samples displayed an enhanced prominence of a cellulose- and hemicellulose-related peak (1730 cm^{-1}), indicating the removal of lignin.

3.3. Thermal Stability

The pristine wood presented a typical gradual weight loss in the temperature range corresponding to the decomposition of wood components, with major weight loss attributed to the breakdown of cellulose, hemicellulose, and lignin (Figure 3). Besides, the DTG curve displays sharp peaks corresponding to the decomposition of different wood components, with distinct peaks for cellulose, hemicellulose, and lignin degradation. This thermal decomposition profile is normally divided into three stages. The initial phase takes place within a lower temperature span (20–100 °C), primarily linked to the expulsion of adsorbed and absorbed water molecules alongside volatile substances. The subsequent phase demonstrates a substantial mass reduction (approximately 70%), corresponding to the devolatilization phenomena related to wood polysaccharides manifesting between 300 and 400 °C. The ultimate stage involves a gradual mass decrement, occurring within the temperature range of 250–500 °C, attributed to the gradual decomposition of lignin. A comprehensive elucidation of this thermal progression was put forth by [51].

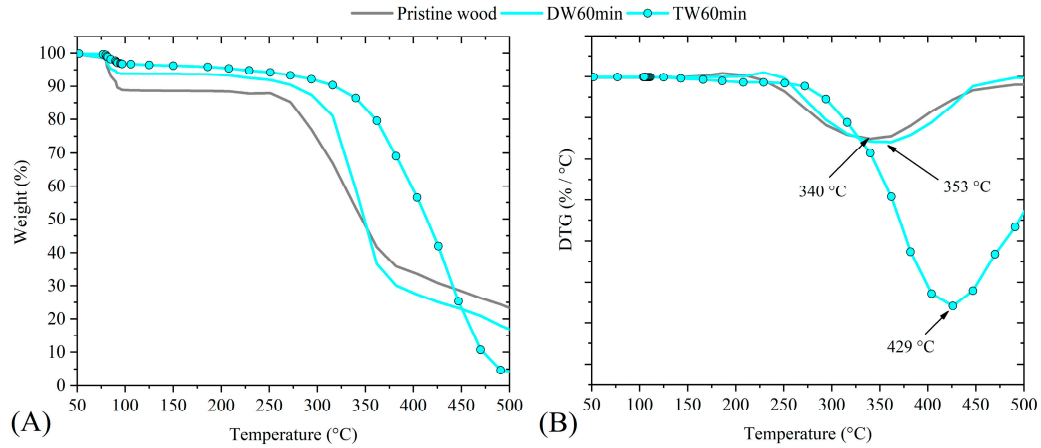

Figure 3. (**A**) and (**B**) show, respectively, the loss of mass in relation to temperature and the derivative of the loss of mass in relation to time for pristine wood, delignified wood for 60 min and transparent wood that was delignified for 60 min.

The delignified sample exhibited a decreased weight loss within the temperature range of 120–350 °C, attributed to the lignin removal. This led to a smoother and earlier decomposition profile compared to the pristine wood. Additionally, the DTG peak observed at 340 °C for the pristine sample shifted to 353 °C for the delignified one, suggesting the absence of significant lignin-related peaks. These findings are consistent with previous research on delignification's impact on thermal properties [8,52].

Moving to the transparent wood, distinct weight loss stages associated with the decomposition of wood components and PMMA impregnation were not discernible, possibly due to overlapping effects. This aligns with the findings in the literature that note the challenge of distinguishing between individual weight loss stages when multiple components are involved. The absence of a clear differentiation might stem from the complex

interaction between the wood components and impregnated polymers, influencing the thermal degradation process.

The primary thermal event indicated by the shift of the DTG peak from 353 °C to 429 °C in the delignified wood upon PMMA impregnation confirms the presence of PMMA. This shift can be attributed to the interactions between PMMA and the wood structure, affecting the thermal behavior. Previous studies suggest that the presence of polymers can lead to shifts in the thermal degradation peaks, emphasizing the influence of the impregnation materials on the thermal properties of wood [8].

3.4. Hygroscopic Characteristics

Figure 4 illustrates the apparent contact angle dynamics over a period of 60 s. In the case of the pristine wood, the initial contact angle was relatively high, measuring around 120°. However, this angle consistently decreased over time, reaching nearly 0° at approximately 55 s. This decrease in contact angle can be attributed to the wood's surface becoming more hydrophilic as water molecules were progressively absorbed into the porous structure. This phenomenon aligns with prior research that highlights the wettability of wood surfaces due to capillary action and the interaction of water with cell wall components [53].

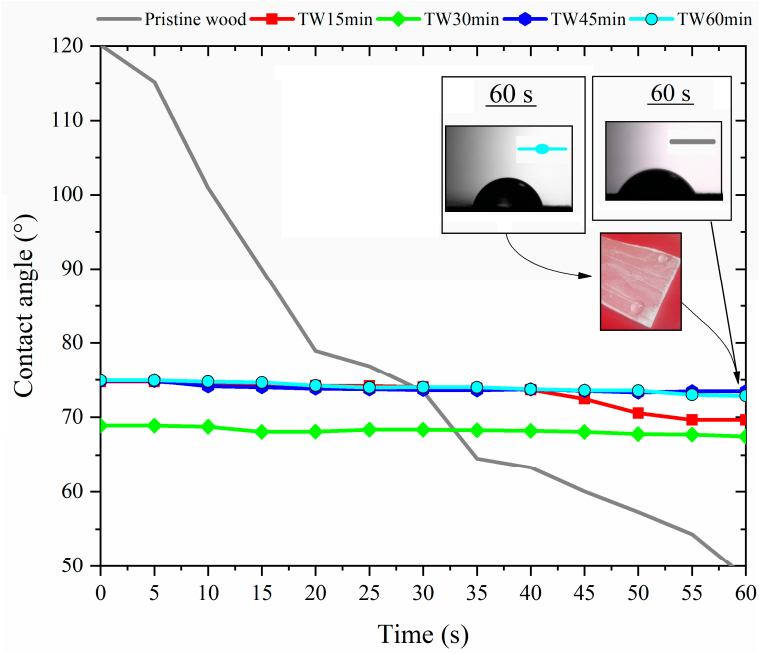

Figure 4. Contact angle results of the pristine and transparent woods.

Conversely, the transparent woods, produced through various delignification durations, exhibited minimal variations in the evolution of contact angles. Despite differences in the delignification times, the contact angles remained within a relatively narrow range of 75–68° across all the samples. Such stability can be attributed to the uniform distribution of the impregnating polymer, which can act as a protective layer on the wood's surface. Studies suggest that polymer impregnation can alter the surface chemistry of wood, affecting its interaction with liquids and consequently stabilizing contact angles [9].

The WRE data (shown in Figure 5) exhibit the same pattern as the contact angle, indicating no significant differences in the comparison between the means obtained from different cycles, nor even in a comparison among the different types of transparent wood. The congruence between the WRE and contact angle data underscores the reliability and reproducibility of transparent wood's surface modifications. This consistency opens doors for utilizing transparent wood in diverse technological applications, where controlled surface interactions play a crucial role in material performance.

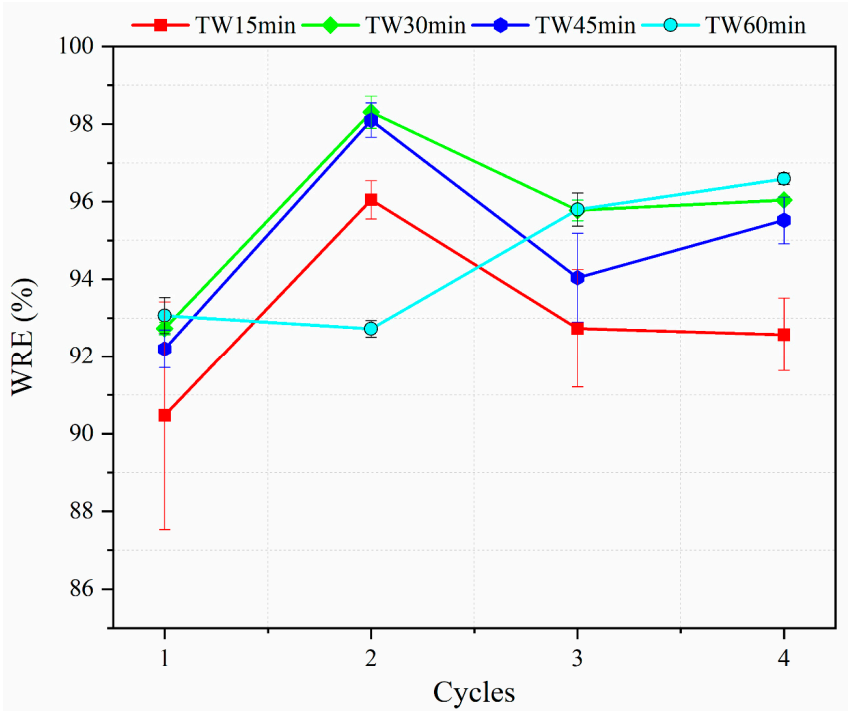

Figure 5. Water repellence efficiency (WRE) data for the transparent woods.

3.5. Mechanical Properties

Regarding the results concerning the tensile mechanical properties (Figure 6), there was a gradual reduction in the properties of the transparent woods as a function of the delignification time, except for the wood delignified for the longest duration (60 min), which exhibited mechanical properties similar to the pristine wood lamina (non-delignified). These properties are higher than those found in the literature [19,45,47,54].

The observed trend in decreasing tensile mechanical properties in the transparent woods as the delignification time increases can be attributed to the removal of lignin. Lignin serves as a binding material in the wood's cell wall structure, providing mechanical strength and rigidity. Studies have indicated that the removal of lignin leads to a decrease in the load-bearing capacity of the wood [55,56]. As the wood's structural integrity is compromised through delignification, its ability to withstand mechanical stress, such as tension, gradually diminishes.

Conversely, the transparent wood sample delignified for the longest duration displaying mechanical properties to the pristine wood lamina suggests that a critical point might have been reached where further delignification does not yield substantial benefits in terms of mechanical performance. This could be due to the presence of other wood components, such as cellulose and hemicellulose, which contribute to the material's mechanical properties. The preservation of these components, even in the face of extensive delignification, could explain the relatively unchanged mechanical behavior [57]. The advantage of transparent wood over pristine wood for structural applications, in addition to the transparency given to the material, is the ductility associated with the calculated toughness, since the work to fracture is higher for TW60min. Studies have indicated that the high work to fracture is mainly caused by the intrinsic properties of the polymer, the complex hierarchical structure of the wood, and the effects of the composite material in the form of new hardening mechanisms [58].

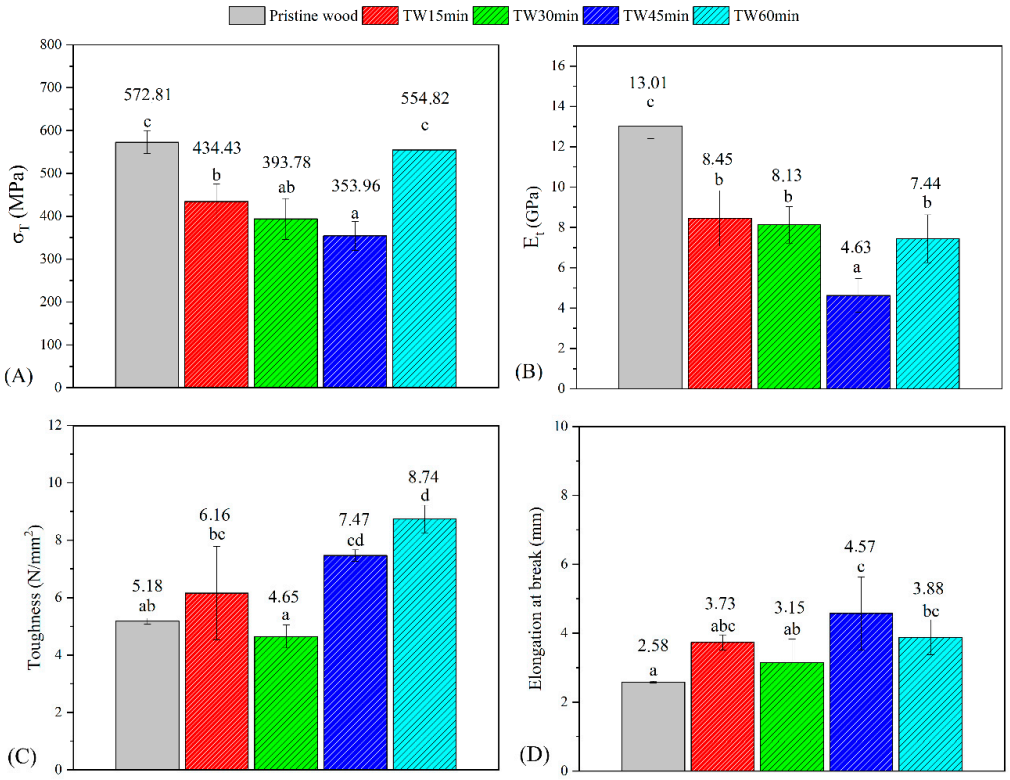

Figure 6. Tensile strength (**A**), tensile modulus (**B**), toughness (**C**), and elongation at break (**D**) data for the pristine wood and transparent woods where E_t is the tensile modulus and σ_t is the tensile strength. Where: Different letters above the deviations represent statistical differences between the groups according to ANOVA.

3.6. Surface Roughness

In terms of surface roughness (Figure 7), both the pristine wood and the wood delignified for 15 min demonstrated the highest mean values of Ra and Rz. In contrast, the woods subjected to longer delignification periods (30, 45, and 60 min) exhibited reduced levels of surface roughness, with similar values observed across these samples.

The higher surface roughness observed in the original wood and the wood delignified for 15 min can be attributed to the presence of lignin and other cell wall components. Lignin, being a relatively rigid and irregular polymer, can contribute to surface irregularities. Moreover, the cell wall's natural structure, which consists of various components with differing mechanical properties, can result in variations in surface roughness. Prior research has established that the presence of lignin and cellulose fibrils can contribute to a higher surface roughness in wood samples [20,25].

The decrease in the surface roughness observed in the woods delignified for longer periods aligns with the concept that delignification tends to result in smoother surfaces. The removal of lignin, which often protrudes from the wood surface, can lead to a more uniform and smoother surface [59,60]. This effect becomes more prominent as delignification progresses and lignin is progressively removed from the wood's structure. Additionally, during the impregnation process, the surface of the transparent wood is coated with an ultrafine layer of PMMA [61].

The convergence of the surface roughness values among the woods delignified for longer durations suggests that beyond a certain point, further delignification might not significantly impact the surface roughness. This could be due to the fact that after extensive delignification, the remaining wood components have a more consistent impact on the surface topography [62].

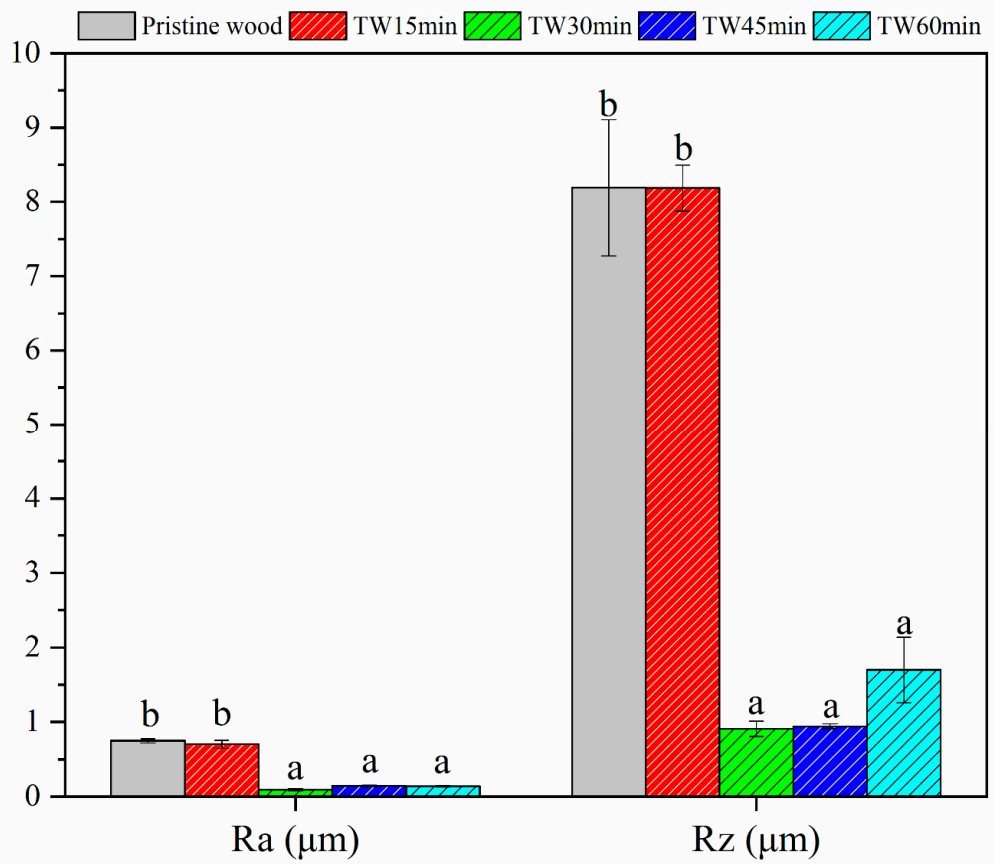

Figure 7. Average roughness (Ra) and average distance between the peak and valley (Rz) for the pristine and transparent woods. Where: Different letters above the deviations represent statistical differences between the groups according to ANOVA.

3.7. Optical Characteristics

Compared to the pristine wood, most variations in light absorption and transmission for the UV-Vis spectra of the transparent woods delignified for 15 min and 30 min can be ascribed to the removal of lignin, although slight changes in the wavelength range could also indicate the interaction between the wood and PMMA. Conversely, the transparent woods delignified for 45 min and 60 min presented further increases in the differences in the UV-VIS spectra (especially in the 300–550 cm^{-1} wavelength range) which could be observed, indicating more substantial interaction between the eucalyptus wood and the impregnated PMMA. Therefore, the interaction between eucalyptus wood and impregnated PMMA seems to become more evident as lignin is removed, resulting in increased transparency and alterations in the UV-VIS spectra. Previous studies have reported similar results [58,63], and current research shows that transmittance values vary significantly depending on the acrylic polymer used. For example, Wachter et al. [64] found that transmittance did not exceed 70% when using basswood and PMMA in transparent wood studies. Likewise, Liu et al. [65] achieved transmittance values of 70%, consistent with the findings of this study (Figure 8).

There was a trend in the lightening and fading of the wood as its delignification time increased (as shown in Figure 9), which is consistent with the literature [66,67]. These findings are evidenced by the gradual increase in the L* values, accompanied by a gradual decrease in both the a* and b* values.

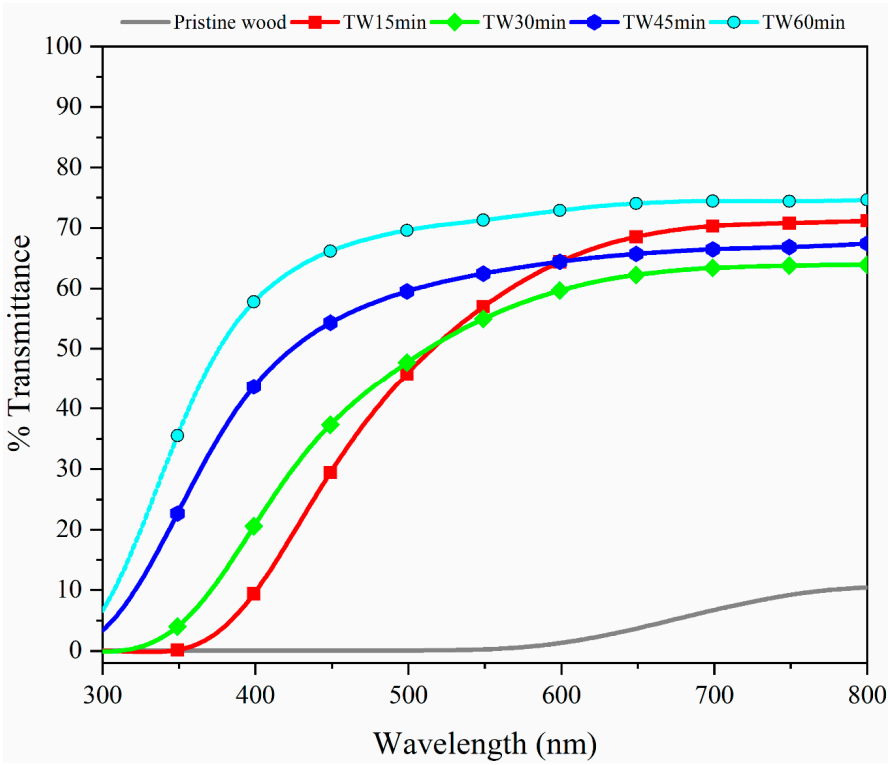

Figure 8. UV-Vis spectra for the pristine and transparent woods.

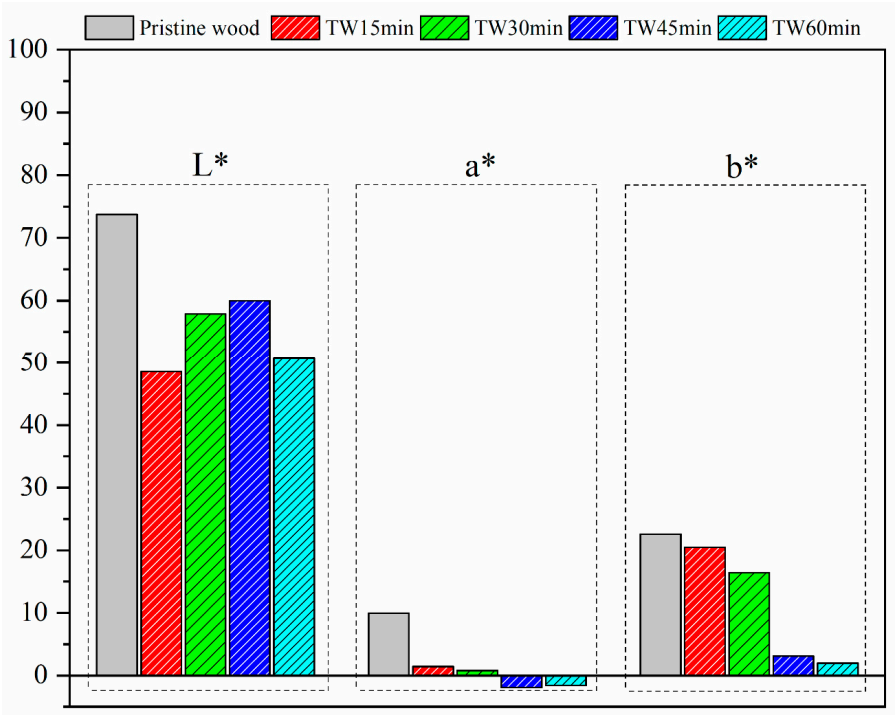

Figure 9. Colorimetric parameters of transparent woods in relation to their delignification time.

This shift in color attributes can be attributed to the removal of lignin, a component responsible for the natural coloration of wood, along with potential alterations in the arrangement and interaction of the wood polymers [37,68]. As lignin diminishes, the wood's inherent lightness becomes more prominent, leading to higher L* values. The reduction in the a* and b* values suggests a decrease in the intensity of the reddish and yellowish hues, contributing to the overall paler appearance.

However, the transparent wood delignified for 60 min stood as an exception and exhibited a higher L* value. Interestingly, there seems to be a correlation between the aforementioned tensile properties and the observation that the transparent wood subjected to extended delignification (60 min) displayed a deeper coloration compared to its counterparts. This contrast is noteworthy, especially considering the prevailing trend in wood lightening with prolonged delignification times. The underlying explanation could be related to the intricate interplay of the wood components. As the delignification process continues, the removal of lignin exposes cellulose and hemicellulose, which could undergo chemical reactions or structural changes leading to the observed darkening effect. This divergence from the anticipated lightning trend underscores the complex nature of wood modification processes and warrants further investigation.

3.8. Morphological Characteristics

During visual observation (Figure 10), the wood samples subjected to different treatment times in the kraft process exhibit distinct transformations. After 15 min, subtle alterations in the transparency and color become discernible, marking the initial stages of the wood's transition towards transparency. At the 30 min mark, the transparency improves further, accompanied by some color shifts (as aforementioned). Following the treatment of 45–60 min, significant enhancements in transparency are evident, accompanied by pronounced color changes, and no substantial differences between these two samples are noticeable.

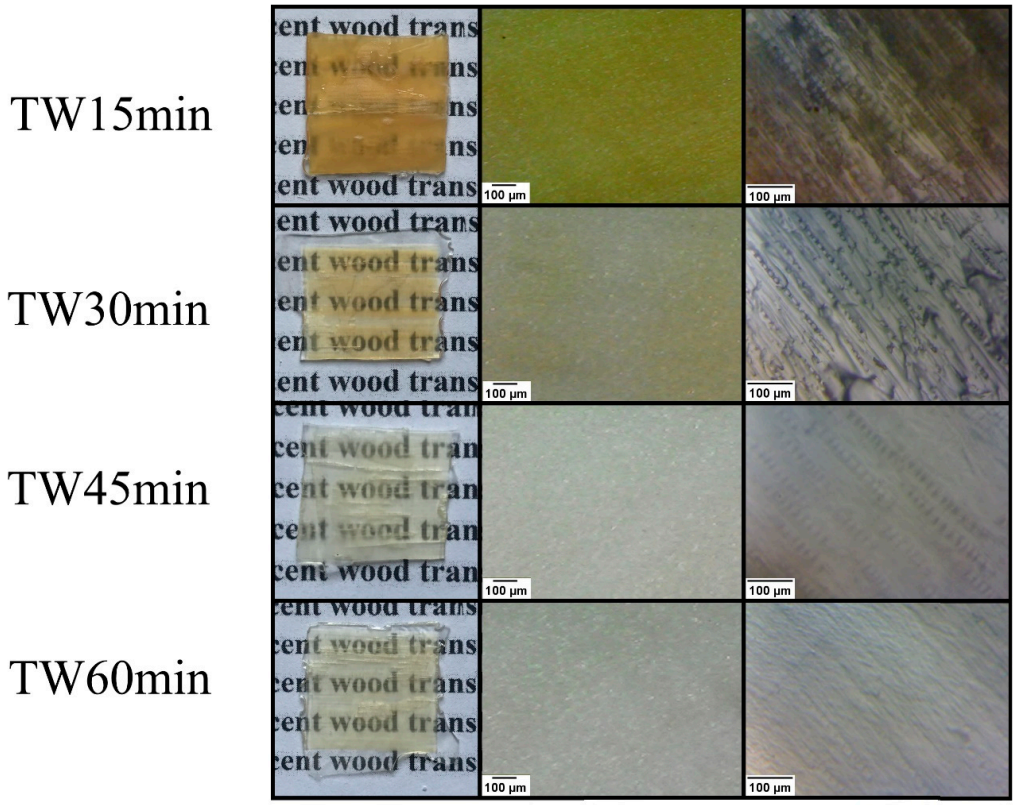

Figure 10. Photographs and optical images of the transparent woods.

The evolving characteristics of the wood samples subjected to different treatment times in the kraft process were also analyzed based on optical images (shown in Figure 11). After 15 min, subtle changes in the transparency and surface texture become apparent, signifying the initial phase of wood modification. Additionally, the wood's initial brownish coloration might shift towards a more yellowish hue. Continuing for 30 min, the transparency advances, and the cellular structure changes become more discernible, accompanied by

a transition from a brownish coloration to a yellowish tint. Extending the treatment time to 45–60 min, notable shifts in the cellular structure and transparency indicate significant wood modification and successful polymer impregnation.

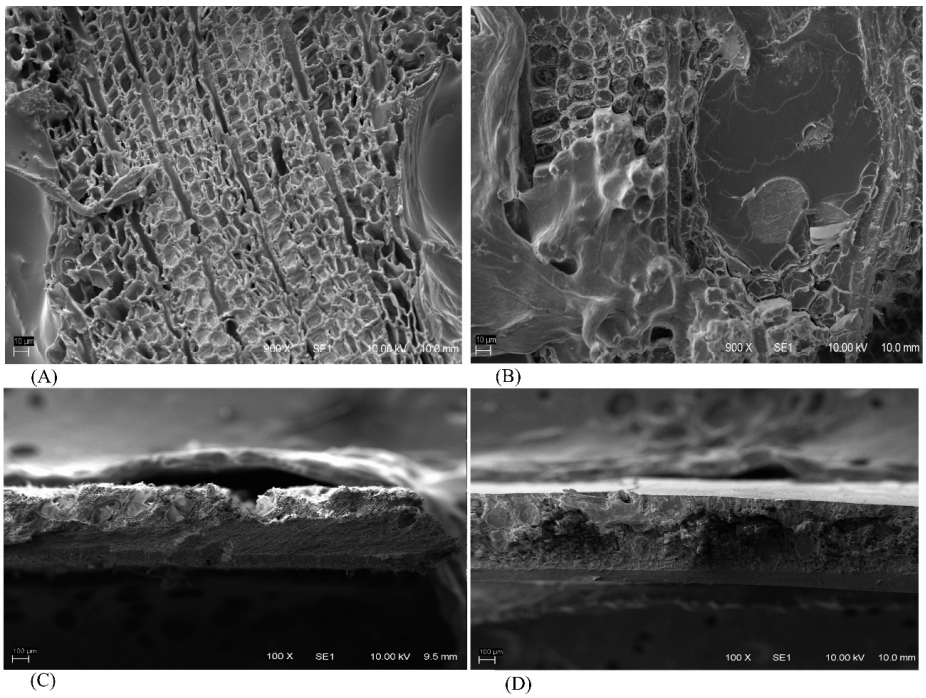

Figure 11. SEM images for the pristine wood (**A**,**C**) and transparent wood called MT60min (**B**,**D**).

The SEM imaging of the MT60min transparent wood sample offers a revealing comparative perspective when contrasted with the original untreated wood. In contrast to the original untreated wood, which exhibits a relatively uniform and intact cellular structure (Figure 11A), the SEM images of the transparent wood sample portray an increased presence of porosity and surface irregularities (Figure 11B). The microstructural alterations signify the ongoing removal of lignin, which contributes to the observed porous regions [20,69]. Additionally, the introduction of polymer impregnation accentuates the shifts in the microstructure, leading to microcracks and variations in the surface texture (Figure 11D), as already reported in the literature [70].

Therefore, based on the SEM analyses, it can be stated that the delignified samples displayed a noticeable increase in porosity, particularly in the regions where lignin was removed. These porous regions correspond to the areas where lignin, which serves as a binding agent in the wood structure, was dissolved during the kraft process. In the transparent wood samples, the impregnation of PMMA into the porous structure resulted in a more homogeneous microstructure, with fewer microcracks and reduced surface irregularities. The presence of PMMA within the wood's cellular structure was evident in the SEM images, indicating a successful polymer impregnation. These micro-morphological changes provide insights into the effectiveness of the delignification and impregnation processes, highlighting the potential of the modified eucalyptus wood for transparent wood applications. The observed microstructural modifications are consistent with the improvements in the mechanical properties and transparency reported in this study.

4. Conclusions

In this study, the application of the kraft process to create transparent wood from Brazilian eucalyptus showcased promising outcomes. Delignification times played a crucial role in influencing thermal stability, compositional changes, and microstructural transformations. As expected, the longer the delignification time, the higher the lignin

removal from the sample, resulting in a delignification percentage of 42.22% at 60 min into the process. Although some studies in the literature have achieved a higher delignification content than that found in this work, the results obtained with the TW60min group have already proven to be satisfactory for obtaining wood with transparency characteristics. Furthermore, the use of this kraft process with eucalyptus wood is innovative, and further research should be conducted to improve this methodology. In this context, the UV-Vis spectroscopy revealed the transition from lignin-rich wood to transparent wood, with distinct absorption bands indicating successful PMMA impregnation. The colorimetric analyses traced the color shifts and transparency, while the microstructural studies depicted the gradual changes in the surface texture and cellular structure. The mechanical properties showed a delicate balance between delignification and mechanical integrity, with critical preservation observed at 60 min of treatment. The surface roughness and wettability analyses indicated changing physical attributes, and visual observations aligned with analytical findings, portraying the progressive nature of transformation. These combined results enhance our understanding of the potential of transparent wood, laying a solid foundation for innovative applications in architecture, design, and sustainable materials. Overall, the kraft pulping process has the potential to stimulate economic growth, create value-added products, and drive sustainable development in Brazil and beyond. These findings pave the way for future research in optimizing process parameters and exploring the effects of varying the chemical composition of raw materials to enhance both the optical properties and overall performance of transparent wood.

Author Contributions: Conceptualization, K.T.B., G.V.C., J.L. and A.P.A.; methodology, K.T.B., G.V.C. and A.P.A.; software, K.T.B., A.P.A. and A.B.A.; validation, K.T.B., A.P.A. and A.B.A.; formal analysis, K.T.B., A.P.A., A.B.A. and R.d.A.D.; investigation, K.T.B., A.P.A. and A.B.A.; resources, R.d.A.D., R.B. and D.A.G.; data curation, K.T.B., A.P.A. and A.B.A.; writing—original draft preparation, K.T.B., A.B.A., J.L. and R.d.A.D.; writing—review and editing, K.T.B., J.L. and R.d.A.D.; visualization, K.T.B. and R.d.A.D.; supervision, R.d.A.D. and R.B.; project administration, R.d.A.D. and R.B.; funding acquisition, D.A.G. and J.L. All authors have read and agreed to the published version of the manuscript.

Funding: This work was supported by Coordination for the Improvement of Higher Education—CAPES (code 001).

Data Availability Statement: Data are contained within the article.

Conflicts of Interest: The authors declare no conflicts of interest.

References

1. Wu, X.; Kong, Z.; Yao, X.; Gan, J.; Zhan, X.; Wu, Y. Transparent Wood with Self-Cleaning Properties for next-Generation Smart Photovoltaic Panels. *Appl. Surf. Sci.* **2023**, *613*, 155927. [CrossRef]
2. Mi, R.; Li, T.; Dalgo, D.; Chen, C.; Kuang, Y.; He, S.; Zhao, X.; Xie, W.; Gan, W.; Zhu, J.; et al. A Clear, Strong, and Thermally Insulated Transparent Wood for Energy Efficient Windows. *Adv. Funct. Mater.* **2020**, *30*, 1907511. [CrossRef]
3. Yaddanapudi, H.S.; Hickerson, N.; Saini, S.; Tiwari, A. Fabrication and Characterization of Transparent Wood for next Generation Smart Building Applications. *Vacuum* **2017**, *146*, 649–654. [CrossRef]
4. Li, Y.; Yang, X.; Fu, Q.; Rojas, R.; Yan, M.; Berglund, L. Towards Centimeter Thick Transparent Wood through Interface Manipulation. *J. Mater. Chem. A* **2018**, *6*, 1094–1101. [CrossRef]
5. Hu, P.; Li, Y.; Zhang, X.; Guo, Z.; Zhang, P. CO_2 Emission from Container Glass in China, and Emission Reduction Strategy Analysis. *Carbon Manag.* **2018**, *9*, 303–310. [CrossRef]
6. Zier, M.; Stenzel, P.; Kotzur, L.; Stolten, D. A Review of Decarbonization Options for the Glass Industry. *Energy Convers. Manag. X* **2021**, *10*, 100083. [CrossRef]
7. Wang, Y.; Wu, Y.; Yang, F.; Yang, L.; Wang, J.; Zhou, J.; Wang, J. A Highly Transparent Compressed Wood Prepared by Cell Wall Densification. *Wood Sci. Technol.* **2022**, *56*, 669–686. [CrossRef]
8. Samanta, P.; Samanta, A.; Montanari, C.; Li, Y.; Maddalena, L.; Carosio, F.; Berglund, L.A. Fire-Retardant and Transparent Wood Biocomposite Based on Commercial Thermoset. *Compos. Part A Appl. Sci. Manuf.* **2022**, *156*, 106863. [CrossRef]
9. Wu, Y.; Wang, Y.; Yang, F. Comparison of Multilayer Transparent Wood and Single Layer Transparent Wood with the Same Thickness. *Front. Mater.* **2021**, *8*, 633345. [CrossRef]

10. Montanari, C.; Ogawa, Y.; Olsén, P.; Berglund, L.A. High Performance, Fully Bio-Based, and Optically Transparent Wood Biocomposites. *Adv. Sci.* **2021**, *8*, 2100559. [CrossRef]
11. Chutturi, M.; Gillela, S.; Yadav, S.M.; Wibowo, E.S.; Sihag, K.; Rangppa, S.M.; Bhuyar, P.; Siengchin, S.; Antov, P.; Kristak, L.; et al. A Comprehensive Review of the Synthesis Strategies, Properties, and Applications of Transparent Wood as a Renewable and Sustainable Resource. *Sci. Total Environ.* **2023**, *864*, 161067. [CrossRef] [PubMed]
12. Li, Y.; Fu, Q.; Rojas, R.; Yan, M.; Lawoko, M.; Berglund, L. Lignin-Retaining Transparent Wood. *ChemSusChem* **2017**, *10*, 3445–3451. [CrossRef]
13. Shi, R.; Sheng, X.; Jia, H.; Zhang, J.; Li, N.; Shi, H.; Niu, M.; Ping, Q. Preparation of Sustainable Transparent Wood with Glucose and Phenol Derived Resin. *Ind. Crops Prod.* **2023**, *193*, 116234. [CrossRef]
14. Wang, M.; Liu, H.; Feng, X.; Wang, X.; Shen, K.; Qi, H.; Rojas, O.J. State-of-the-Art Luminescent Materials Based on Wood Veneer with Superior Strength, Transparency, and Water Resistance. *Chem. Eng. J.* **2023**, *454*, 140225. [CrossRef]
15. Li, Y.F.; Lv, D.J.; Jiang, C.; Liu, Y.X.; Zhang, H.Y. Fabrication and Mechanical Properties of Wood-PMMA Composite. *Adv. Mater. Res.* **2010**, *160–162*, 640–643. [CrossRef]
16. Qian, Y.; Deng, Y.; Li, H.; Qiu, X. Reaction-Free Lignin Whitening via a Self-Assembly of Acetylated Lignin. *Ind. Eng. Chem. Res.* **2014**, *53*, 10024–10028. [CrossRef]
17. Zhang, H.; Bai, Y.; Zhou, W.; Chen, F. Color Reduction of Sulfonated Eucalyptus Kraft Lignin. *Int. J. Biol. Macromol.* **2017**, *97*, 201–208. [CrossRef] [PubMed]
18. Zhu, M.; Li, T.; Davis, C.S.; Yao, Y.; Dai, J.; Wang, Y.; AlQatari, F.; Gilman, J.W.; Hu, L. Transparent and Haze Wood Composites for Highly Efficient Broadband Light Management in Solar Cells. *Nano Energy* **2016**, *26*, 332–339. [CrossRef]
19. Qin, J.; Li, X.; Shao, Y.; Shi, K.; Zhao, X.; Feng, T.; Hu, Y. Optimization of Delignification Process for Efficient Preparation of Transparent Wood with High Strength and High Transmittance. *Vacuum* **2018**, *158*, 158–165. [CrossRef]
20. Wu, J.; Wu, Y.; Yang, F.; Tang, C.; Huang, Q.; Zhang, J. Impact of Delignification on Morphological, Optical and Mechanical Properties of Transparent Wood. *Compos. Part A Appl. Sci. Manuf.* **2019**, *117*, 324–331. [CrossRef]
21. IBÁ. IBÁ Annual Report. *Indústria Bras. Árvores* **2023**, 1–93. Available online: https://www.google.com/url?sa=t&rct=j&q=&esrc=s&source=web&cd=&ved=2ahUKEwi90Yir-5yIAxXxspUCHa2uO6MQFnoECBIQAQ&url=https://iba.org/datafiles/publicacoes/relatorios/relatorio-anual-iba2023-r.pdf&usg=AOvVaw0PSr8vj6V1kdplDnAoqdfW&opi=89978449 (accessed on 28 August 2024).
22. Mboowa, D. A Review of the Traditional Pulping Methods and the Recent Improvements in the Pulping Processes. *Biomass Convers. Biorefinery* **2021**, *14*, 1–12. [CrossRef]
23. Balkissoon, S.; Andrew, J.; Sithole, B. *Dissolving Wood Pulp Production: A Review*; Springer: Berlin/Heidelberg, Germany, 2022; ISBN 0123456789.
24. Gellerstedt, G. Softwood Kraft Lignin: Raw Material for the Future. *Ind. Crops Prod.* **2015**, *77*, 845–854. [CrossRef]
25. Zhu, M.; Song, J.; Li, T.; Gong, A.; Wang, Y.; Dai, J.; Yao, Y.; Luo, W.; Henderson, D.; Hu, L. Highly Anisotropic, Highly Transparent Wood Composites. *Adv. Mater.* **2016**, *28*, 5181–5187. [CrossRef] [PubMed]
26. Van Hai, L.; Muthoka, R.M.; Panicker, P.S.; Agumba, D.O.; Pham, H.D.; Kim, J. All-Biobased Transparent-Wood: A New Approach and Its Environmental-Friendly Packaging Application. *Carbohydr. Polym.* **2021**, *264*, 118012. [CrossRef]
27. De Melo, R.R.; Barbosa, K.T.; Beltrame, R.; Acosta, A.P.; Pimenta, A.S.; Mascarenhas, A.R.P.; Rodolfo de Melo, R.; Barbosa, K.T.; Beltrame, R.; Acosta, A.P.; et al. Ultrasound to Determine Physical-Mechanical Properties of *Eucalyptus camaldulensis* Wood. *Wood Mater. Sci. Eng.* **2021**, *16*, 407–413. [CrossRef]
28. Filho, A.M.; Netto, S.P.; Machado, S.A.; Corte, A.P.; Behling, A. Site Classification for *Eucalyptus* sp. in a Tropical Region of Brazil. *An. Acad. Bras. Cienc.* **2023**, *95*, e20200038. [CrossRef]
29. Mulin, L.B.; Martins, C.C.N.; Dias, M.C.; Santos, A.d.A.d.; Mascarenhas, A.R.P.; Profeti, D.; Oliveira, M.P.; Tonoli, G.H.D.; Moulin, J.C. Effect of Phosphorylation on the Production of Cellulose Nanofibrils from *Eucalyptus* sp. *Ind. Crops Prod.* **2023**, *193*, 116173. [CrossRef]
30. Tappi T257. Sampling and preparing wood for chemical analysis. In *TAPPI TEST METHODS. Technical Association of Pulp an Paper Industry*; Tappi Press: Atlanta, GA, USA, 2012.
31. Tappi T 204 cm-97. Solvent extractives of wood and pulp T 204 cm-97. In *TAPPI TEST METHODS Tech Assoc Pulp an Pap Ind*; Tappi Press: Atlanta, GA, USA, 2012; pp. 1–12.
32. Tappi T222 Om-02. Lignin in wood and pulp. In *TAPPI TEST METHODS. Technical Association of Pulp an Paper Industry*; Tappi Press: Atlanta, GA, USA, 2012; pp. 1–7.
33. Tappi T 211 om-02. Ash in wood, pulp, paper and paperboard: Combustion at 525 °C. In *TAPPI TEST METHODS. Technical Association of Pulp an Paper Industry*; Tappi Press: Atlanta, GA, USA, 2002; pp. 1–5.
34. *ASTM D1003-21*; Standard Test Method for Haze and Luminous Transmittance of Transparent Plastics. Available online: https://www.astm.org/d1003-21.html (accessed on 28 August 2024).
35. *ASTM D638-10*; Standard Test Method for Tensile Properties of Plastics. Available online: https://compass.astm.org/document/?contentCode=ASTM%7CD0638-22%7Cen-US (accessed on 28 August 2024).
36. Resende, J.d.O.; Colodette, J.L.; Andrade, M.F. Estudo de Localização Da Extração Alcalina a Frio (CCE) Numa Sequência de Branqueamento de Polpa Solúvel de Eucalipto. *Sci. For.* **2019**, *47*, 326–335. [CrossRef]

37. Lehr, M.; Miltner, M.; Friedl, A. Removal of Wood Extractives as Pulp (Pre-) Treatment: A Technological Review. *SN Appl. Sci.* **2021**, *3*, 886. [CrossRef]
38. Jiang, Y.; Zeng, X.; Luque, R.; Tang, X.; Sun, Y.; Lei, T.; Liu, S.; Lin, L. Cooking with Active Oxygen and Solid Alkali: A Promising Alternative Approach for Lignocellulosic Biorefineries. *ChemSusChem* **2017**, *10*, 3982–3993. [CrossRef]
39. Martin-sampedro, R.; Eugenio, M.E.; Moreno, J.A.; Revilla, E.; Villar, J.C. Bioresource Technology Integration of a Kraft Pulping Mill into a Forest Biorefinery: Pre-Extraction of Hemicellulose by Steam Explosion versus Steam Treatment. *Bioresour. Technol.* **2014**, *153*, 236–244. [CrossRef] [PubMed]
40. Morais, A.P.d.S.; Sansígolo, C.A.; Neto, M.d.O. Effects of Autohydrolysis of *Eucalyptus urograndis* and *Eucalyptus grandis* on Influence of Chemical Components and Crystallinity Index. *Bioresour. Technol.* **2016**, *214*, 623–628. [CrossRef]
41. Fiskari, J.; Vihelä, T.; Ruuttunen, K.; Ali-Rekola, V.; Hautala, S.; Sixta, H. Cooking of Dry High-Lignin Eucalyptus Camaldulensis Chips Followed by TCF Bleaching with Hydrogen Peroxide. *Cellul. Chem. Technol.* **2017**, *51*, 857–861.
42. Abad, S.; Santos, V.; Parajó, J.C. Evaluation of *Eucalyptus globulus* Wood Processing in Media Made up of Formic Acid, Water, and Hydrogen Peroxide for Dissolving Pulp Production. *Ind. Eng. Chem. Res.* **2001**, *40*, 413–419. [CrossRef]
43. Isaza Ferro, E.; Ruuttunen, K.; Perrin, J.; Vuorinen, T. Sustainable Bleaching of *Eucalyptus* sp. Kraft Pulp with Hypochlorous Acid, Ozone and Hydrogen Peroxide. *Ind. Crops Prod.* **2021**, *172*, 114004. [CrossRef]
44. Pinto, P.C.; Evtuguin, D.V.; Neto, C.P.; Silvestre, A.J.D.; Amado, F.M.L. Behavior of *Eucalyptus globulus* lignin during kraft pulping. II. analysis BY NMR, ESI/MS, AND GPC. *J. Wood Chem. Technol.* **2002**, *22*, 109–125. [CrossRef]
45. Jungstedt, E.; Montanari, C.; Östlund, S.; Berglund, L. Mechanical Properties of Transparent High Strength Biocomposites from Delignified Wood Veneer. *Compos. Part A Appl. Sci. Manuf.* **2020**, *133*, 105853. [CrossRef]
46. Li, Y.; Fu, Q.; Yu, S.; Yan, M.; Berglund, L. Optically Transparent Wood from a Nanoporous Cellulosic Template: Combining Functional and Structural Performance. *Biomacromolecules* **2016**, *17*, 1358–1364. [CrossRef]
47. Wu, Y.; Wu, J.; Yang, F.; Tang, C.; Huang, Q. Effect of H_2O_2 Bleaching Treatment on the Properties of Finished Transparent Wood. *Polymers* **2019**, *11*, 776. [CrossRef]
48. Muhammad, N.A.; Armynah, B.; Tahir, D. High Transparent Wood Composite for Effective X-ray Shielding Applications. *Mater. Res. Bull.* **2022**, *154*, 111930. [CrossRef]
49. Sternberg, J.; Pilla, S. Materials for the Biorefinery: High Bio-Content, Shape Memory Kraft Lignin-Derived Non-Isocyanate Polyurethane Foams Using a Non-Toxic Protocol. *Green Chem.* **2020**, *22*, 6922–6935. [CrossRef]
50. Varnagirytė-Kabašinskienė, I.; Pukalskienė, M.; Šilinskas, B.; Škėma, M.; Aleinikovas, M. Physical and Chemical Changes in Hydrothermally Modified Wood. *Forests* **2021**, *12*, 1771. [CrossRef]
51. Arâmburu, A.; Lunkes, N.; de Cademartori, P.H.G.; Gatto, D.A.; Missio, A.L.; Delucis, R.A. Forestry Wastes: Technical Concepts, Economic Circularity, and Sustainability Approaches. In *Handbook of Waste Biorefinery*; Springer International Publishing: Cham, Switzerland, 2022; pp. 369–415.
52. Ding, L.; Han, X.; Chen, L.; Jiang, S. Preparation and Properties of Hydrophobic and Transparent Wood. *J. Bioresour. Bioprod.* **2022**, *7*, 295–305. [CrossRef]
53. Acosta, A.P.; Barbosa, K.T.; Amico, S.C.; Missio, A.L.; de Avila Delucis, R.; Gatto, D.A. Improvement in Mechanical, Physical and Biological Properties of Eucalyptus and Pine Woods by Raw Pine Resin in Situ Polymerization. *Ind. Crops Prod.* **2021**, *166*, 113495. [CrossRef]
54. Qiu, Z.; Xiao, Z.; Gao, L.; Li, J.; Wang, H.; Wang, Y.; Xie, Y. Transparent Wood Bearing a Shielding Effect to Infrared Heat and Ultraviolet via Incorporation of Modified Antimony-Doped Tin Oxide Nanoparticles. *Compos. Sci. Technol.* **2019**, *172*, 43–48. [CrossRef]
55. Mi, R.; Chen, C.; Keplinger, T.; Pei, Y.; He, S.; Liu, D.; Li, J.; Dai, J.; Hitz, E.; Yang, B.; et al. Scalable Aesthetic Transparent Wood for Energy Efficient Buildings. *Nat. Commun.* **2020**, *11*, 3836. [CrossRef] [PubMed]
56. Fu, Q.; Yan, M.; Jungstedt, E.; Yang, X.; Li, Y.; Berglund, L.A. Transparent Plywood as a Load-Bearing and Luminescent Biocomposite. *Compos. Sci. Technol.* **2018**, *164*, 296–303. [CrossRef]
57. Wu, Y.; Wang, J.; Wang, Y.; Zhou, J. Properties of Multilayer Transparent Bamboo Materials. *ACS Omega* **2021**, *6*, 33747–33756. [CrossRef]
58. Li, Y.; Vasileva, E.; Sychugov, I.; Popov, S.; Berglund, L. Optically Transparent Wood: Recent Progress, Opportunities, and Challenges. *Adv. Opt. Mater.* **2018**, *6*, 1800059. [CrossRef]
59. Jacucci, G.; Schertel, L.; Zhang, Y.; Yang, H.; Vignolini, S. Light Management with Natural Materials: From Whiteness to Transparency. *Adv. Mater.* **2021**, *33*, 2001215. [CrossRef] [PubMed]
60. Parit, M.; Du, H.; Zhang, X.; Jiang, Z. Flexible, Transparent, UV-Protecting, Water-Resistant Nanocomposite Films Based on Polyvinyl Alcohol and Kraft Lignin-Grafted Cellulose Nanofibers. *ACS Appl. Polym. Mater.* **2022**, *4*, 3587–3597. [CrossRef]
61. Zhou, J.; Xu, W. Toward Interface Optimization of Transparent Wood with Wood Color and Texture by Silane Coupling Agent. *J. Mater. Sci.* **2022**, *57*, 5825–5838. [CrossRef]
62. Kundu, C.; Samudrala, S.P.; Kibria, M.A.; Bhattacharya, S. One-Step Peracetic Acid Pretreatment of Hardwood and Softwood Biomass for Platform Chemicals Production. *Sci. Rep.* **2021**, *11*, 11183. [CrossRef] [PubMed]
63. Zhang, J.; Koubaa, A.; Tao, Y.; Li, P.; Xing, D. The Emerging Development of Transparent Wood: Materials, Characteristics, and Applications. *Curr. For. Rep.* **2022**, *8*, 333–345. [CrossRef]

64. Wachter, I.; Štefko, T.; Rantuch, P.; Martinka, J.; Pastierová, A. Effect of UV Radiation on Optical Properties and Hardness of Transparent Wood. *Polymers* **2021**, *13*, 2067. [CrossRef]
65. Liu, Y.; Zhang, Y.; Guo, J.; Guo, G.; Li, C. Preparation and Properties of Soft-/Hard-Switchable Transparent Wood with 0 °C as a Boundary. *Forests* **2024**, *15*, 384. [CrossRef]
66. Wu, Y.; Zhou, J.; Huang, Q.; Yang, F.; Wang, Y.; Liang, X.; Li, J. Study on the Colorimetry Properties of Transparent Wood Prepared from Six Wood Species. *ACS Omega* **2020**, *5*, 1782–1788. [CrossRef]
67. Subba Rao, A.N.; Nagarajappa, G.B.; Nair, S.; Chathoth, A.M.; Pandey, K.K. Flexible Transparent Wood Prepared from Poplar Veneer and Polyvinyl Alcohol. *Compos. Sci. Technol.* **2019**, *182*, 107719. [CrossRef]
68. Lesar, B.; Pavlič, M.; Petrič, M.; Škapin, A.S.; Humar, M. Wax Treatment of Wood Slows Photodegradation. *Polym. Degrad. Stab.* **2011**, *96*, 1271–1278. [CrossRef]
69. Höglund, M.; Johansson, M.; Sychugov, I.; Berglund, L.A. Transparent Wood Biocomposites by Fast UV-Curing for Reduced Light-Scattering through Wood/Thiol–Ene Interface Design. *ACS Appl. Mater. Interfaces* **2020**, *12*, 46914–46922. [CrossRef]
70. Arcieri, N.; Chen, B.; Berglund, L.A.; Tavares da Costa, M.V. Crack Growth Study of Wood and Transparent Wood-Polymer Composite Laminates by in-situ Testing in Weak TR-Direction. *Compos. Part A Appl. Sci. Manuf.* **2023**, *173*, 107693. [CrossRef]